MABS
2022, VOL. 14, NO. 1, e2013750 (12 pages)
https://doi.org/10.1080/19420862.2021.2013750

Taylor & Francis
Taylor & Francis Group

REPORTS

OPEN ACCESS Check for updates

Structural and functional characterization of a monoclonal antibody blocking TIGIT

Bo-Seong Jeong[a,$], Hyemi Nam[b,$], Jeewon Lee[b], Hye-Young Park[b], Ki Joon Cho[b], Joong Hyuk Sheen[b,#], Eunjung Song[c], Meesook Oh[d], Sunggeun Lee[d], Hyemin Choi[d], Jung-Eun Yang[d], Munkyung Kim[b], and Byung-Ha Oh[a]

[a]Department of Biological Sciences, Kaist Institute for the Biocentury, Korea Advanced Institute of Science and Technology, Daejeon, Republic of Korea; [b]Department of Target ID & Assay Development, Mogam Institute for Biomedical Research, Gyeonggi-do, Republic of Korea; [c]Department of Protein Engineering, Mogam Institute for Biomedical Research, Gyeonggi-do, Republic of Korea; [d]Department of Research and Early Development, Gc Pharma, Gyeonggi-do, Republic of Korea

ABSTRACT

TIGIT is an immune checkpoint receptor that is expressed on subsets of activated T cells and natural killer (NK) cells. Several ligands for TIGIT, including poliovirus receptor (PVR), are expressed on cancer cells and mediate inhibitory signaling to suppress antitumor activities of the immune cells. Many studies support that the TIGIT signaling is a potential target for cancer immunotherapy. We developed an IgG4-type monoclonal antibody against human TIGIT, designated as MG1131, using a phage display library of single-chain variable fragments (scFvs). MG1131 interacts with TIGIT much more tightly than PVR does. The crystal structure of a scFv version of MG1131 bound to TIGIT was determined, showing that MG1131 could block the PVR-TIGIT interaction and thus the immunosuppressive signaling of TIGIT. Consistently, MG1131 is bound to TIGIT-expressing cells and interferes with PVR binding to these cells. Moreover, MG1131 increased NK cell-mediated tumor killing activities, inhibited immunosuppressive activity of regulatory T (Treg) cells from healthy donors, and restored interferon-γ secretion from peripheral blood mononuclear cells derived from multiple myeloma patients. MG1131 also increased T cell infiltration to the tumor site and inhibited tumor growth in mice. Collectively, these data indicate that MG1131 modulates the effector functions of T cells and NK cells positively and Treg cells negatively.

ARTICLE HISTORY
Received 18 July 2021
Revised 10 November 2021
Accepted 30 November 2021

KEYWORDS
Cancer; immune checkpoint; TIGIT; monoclonal antibody; crystal structure

Introduction

TIGIT is an immunosuppressive receptor that is expressed on $CD8^+$ T cells, $CD4^+$ T cells, Treg cells, and natural killer (NK) cells.[1–3] It is composed of an extracellular Ig variable domain, a single-pass transmembrane segment, and a cytoplasmic region that contains an immunoglobulin tail tyrosine (ITT)-like motif and an immunoreceptor tyrosine-based inhibitory motif (ITIM).[1,2,4] Upon phosphorylation, the ITT-like motif recruits Grb2 and the tyrosine phosphatase SHIP, which is a key inhibitor of phosphoinositide 3-kinase signaling.[5] The role of ITIM in TIGIT is obscure.[6] Poliovirus receptor (PVR; also known as CD155) and Nectin-2 (also known as CD112) are the two major physiological ligands of TIGIT that are expressed on antigen-presenting cells (APCs) and many human malignant tumors.[7–9] Their binding to TIGIT induces immunosuppressive and regulatory profiles in NK cells and T cells.[10,11] Structural and biochemical studies suggested that TIGIT and PVR form a cis-trans signaling cluster on the cell surface where TIGIT homodimers and PVR homodimers heterodimerize in trans in a zipper-like array.[12]

PVR and Nectin-2 also recognize DNAM-1 (DNAX accessory molecule 1; CD226), a co-stimulatory receptor expressed on most immune cells.[13,14] Their binding to DNAM-1 induces immune cell activation and cytotoxicity of effector T cells.[15,16] Notably, the binding affinity of PVR and Nectin-2 for TIGIT is higher than that for DNAM-1, indicating that they would preferentially interact with TIGIT and thus tumor-infiltrating lymphocytes (TILs) would be skewed toward immunosuppressed phenotypes.[17] These and other supporting data highlighted TIGIT as a major emerging target for immunotherapy. Subsequently, blocking TIGIT using anti-TIGIT monoclonal antibodies (mAbs) demonstrated effective antitumor or antiviral responses.[18–23] Currently, various formats involving an anti-TIGIT mAb are under preclinical investigation or in clinical trials.[24] Tiragolumab, one of the most advanced anti-TIGIT mAbs in clinical development, has shown encouraging efficacy in non-small cell lung cancer patients in combination with the anti-PD-L1 mAb, atezolizumab, in a Phase 2 clinical trial.[25] However, there has been no report on any anti-TIGIT mAb whose molecular interaction has been structurally characterized.

We have developed an IgG4-type mAb against human TIGIT (hTIGIT), named MG1131, which binds to hTIGIT with much higher affinity than PVR does. We show that MG1131 augments NK cell-mediated tumor-killing activities in a PVR-dependent manner and suppresses the activity of Treg cells *in vitro*. Furthermore, MG1131 elicited anti-tumor activity in both the hTIGIT knock-in (KI) mouse model and the human colon cancer-derived xenograft mouse model.

CONTACT Byung-Ha Oh bhoh@kaist.ac.kr; Munkyung Kim munkyung2@gmail.com Department of Biological Sciences, Kaist Institute for the Biocentury, Korea Advanced Institute of Science and Technology, Daejeon, Republic of Korea
[#]*Present address: Translational Immunology, BioNTech, Cambridge, MA, USA*
[$]These authors contributed equally to this work.

Biochemical characterization and anti-tumoral activities of MG1131 are presented along with the crystal structure of an scFv of MG1131 (MG1131-scFv) bound to the ectodomain of hTIGIT at 1.5 Å resolution, which provides structural bases for the *in vitro* and *in vivo* properties of MG1131.

Results

Discovery, development, and characterization of MG1131

A total of 11 candidate antibodies against hTIGIT were chosen from a phage display library and subjected to experimental screening. Three clones, MG1131, WINB6, and WIND2, were chosen from the initial screening based on their high TIGIT-binding affinity (Figure 1a and Table 1) and high potency of blocking PVR binding to Jurkat T cells stably expressing hTIGIT (hTIGIT-Jurkat cells) (Figure 1b and Table 1). To select the final candidate, we compared the blockade of the TIGIT-PVR interaction by these antibodies using a luciferase reporter assay. Two cell lines were used in this assay: 1) Jurkat T cells expressing hTIGIT and a luciferase reporter driven by a native response element (TIGIT effector cells) and 2) Chinese hamster ovary (CHO)-K1 cells expressing human PVR and a T cell receptor (TCR)-activating protein (hPVR-aAPC/CHO-K1). The two cell lines were co-cultured in the presence of each of these anti-TIGIT mAbs, and the potency in the activation of TIGIT effector cells was measured by the luciferase activity. MG1131 demonstrated superior T cell activation compared with WIND2, WINB6, and 1D3, the in-house version of tiragolumab used as a reference mAb (Figure 1c). Based on these data, MG1131 was selected as the final lead molecule.

Before further analyses, we constructed MG1131 into an IgG4-type mAb to avoid potential death of NK or T cells by IgG1-type mAb via the effector function of its Fc domain. 1D3 was also constructed in the same type. We first measured and compared the binding affinities of MG1131 and 1D3 for hTIGIG (22–141), the ectodomain of the protein, by biolayer interferometry (BLI). In this experiment, which essentially evaluated the bivalent interaction of the mAbs with the antigen, MG1131

Table 1. Cell-based binding assay and competition assay.

	Binding to hTIGIT-Jurkat cell	Competition with PVR-Fc
Antibodies	EC_{50} (μg/ml)	IC_{50} (μg/ml)
MG1131	0.017	0.093
1B11	0.041	0.285
1 C3	0.053	0.398
1E12	0.068	0.236
1E4	0.015	0.082
1F2	0.017	0.143
1F10	0.080	0.380
WINB6	0.016	0.068
WINB11	0.021	0.076
WIND2	0.017	0.071
E8_2nd	0.021	0.102

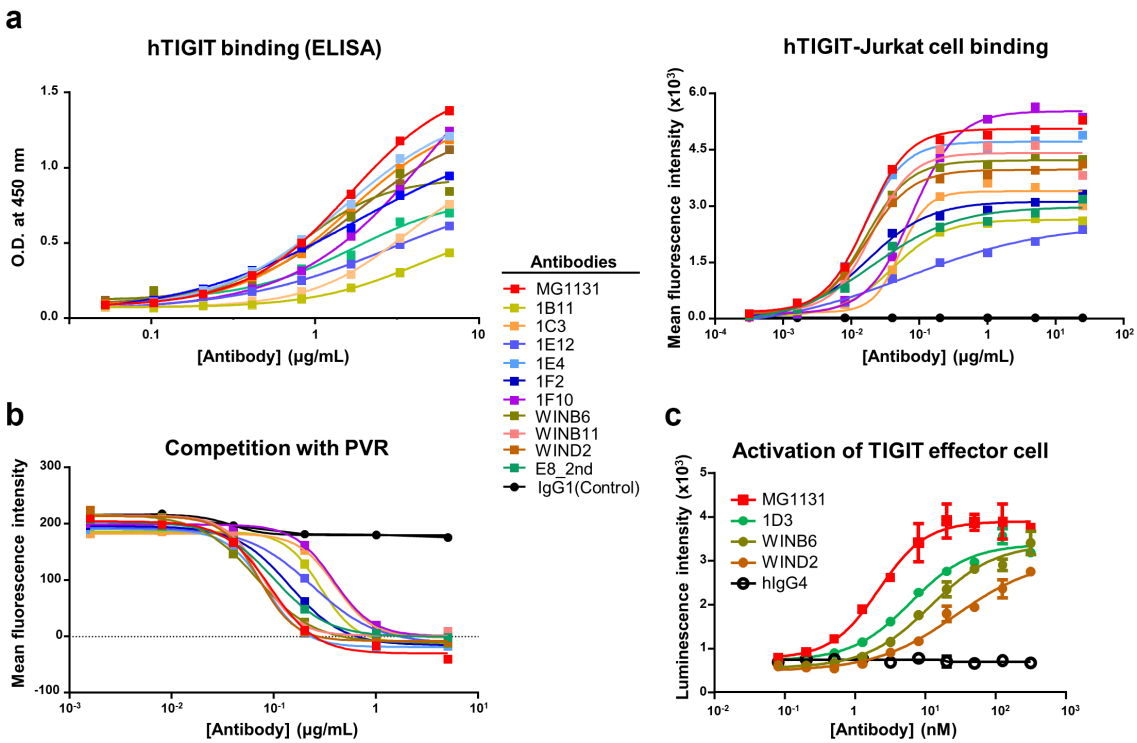

Figure 1. Screening of anti-hTIGIT antibodies selected from a phage display library. (A) hTIGIT-binding affinity. Eleven selected antibodies (IgG1 type) were analyzed for their binding interaction with hTIGIT by ELISA and by a cell-based assay using hTIGIT-Jurkat cells. EC_{50} is the antibody concentration at which 50% of maximal fluorescence intensity is achieved (Table 1).(B) Competition assay. hTIGIT-Jurkat cells were pretreated with PVR-Fc (50 μg/mL) and exposed to varying concentrations of the antibodies. After washing, the remaining PVR-Fc were detected by PE-conjugated anti-PVR antibody. IC_{50} is the antibody concentration at which 50% reduction of the fluorescence intensity is achieved (Table 1).(C) Luciferase reporter assay. TIGIT effector cells and CHO-K1 cells were co-cultured with the four indicated antibodies at varying concentrations. Activation of TIGIT effector cells was measured by the luciferase activity. N = 2.Figure 1a Alt text: (Left) Eleven selected antibodies were tested for their binding to the target protein (hTIGIT) in solution, and the line graph shows their binding signal as a function of the antibody concentration. (Right) Similarly, their binding to the cells expressing hTIGIT on the cell surface were measured and plotted.Figure 1b Alt text: Eleven selected antibodies were tested for their potency in competing with a natural ligand (PVR) for binding to hTIGIT-expressing cells. Reduction of PVR binding to the cell is plotted as a function of their concentration.Figure 1c Alt text: Three selected antibodies were tested for their ability to activate effector cells. A line graph shows that MG1131 exhibited the highest activity.

exhibited an apparent dissociation constant (K_D) of 2.1 pM. This potent binding affinity was better than that of 1D3 (K_D of 8.1 pM) (Figure 2a). We evaluated the monovalent interaction of MG1131 by producing the antigen-binding fragment (Fab) form (MG1131-Fab) and measuring the binding affinity by the same BLI experiment to find that MG1131-Fab binds to hTIGIT(22–141) with the K_D of 2.2 nM (Figure 2a). This tight monovalent interaction explains the potent bivalent interaction of MG1131. Subsequent cell-based binding experiments showed that MG1131 binds to hTIGIT-Jurkat cells, peripheral blood mononuclear cell (PBMC)-derived NK cells and Treg cells with EC_{50} values of 0.024 μg/mL, 0.035 μg/mL and 0.018 μg/mL, respectively, which were lower or at least comparable to that of 1D3 (Figure 2b). A competition assay using hTIGIT-Jurkat cells pre-treated with recombinant PVR-Fc showed that MG1131 efficiently inhibited PVR-Fc binding to the cells with IC_{50} of 0.246 μg/mL, presumably by competing with PVR-Fc for binding to TIGIT on the cell surface (Figure 2c). In these experiments, MG1131 exhibited better or at least comparable activities in comparison with 1D3, which is consistent with the binding affinity measurement. Of note, neither MG1131 nor 1D3 exhibited any considerable binding to Jurkat cells, which do not express TIGIT (Figure 2b), indicating good target specificity of MG1131 and 1D3.

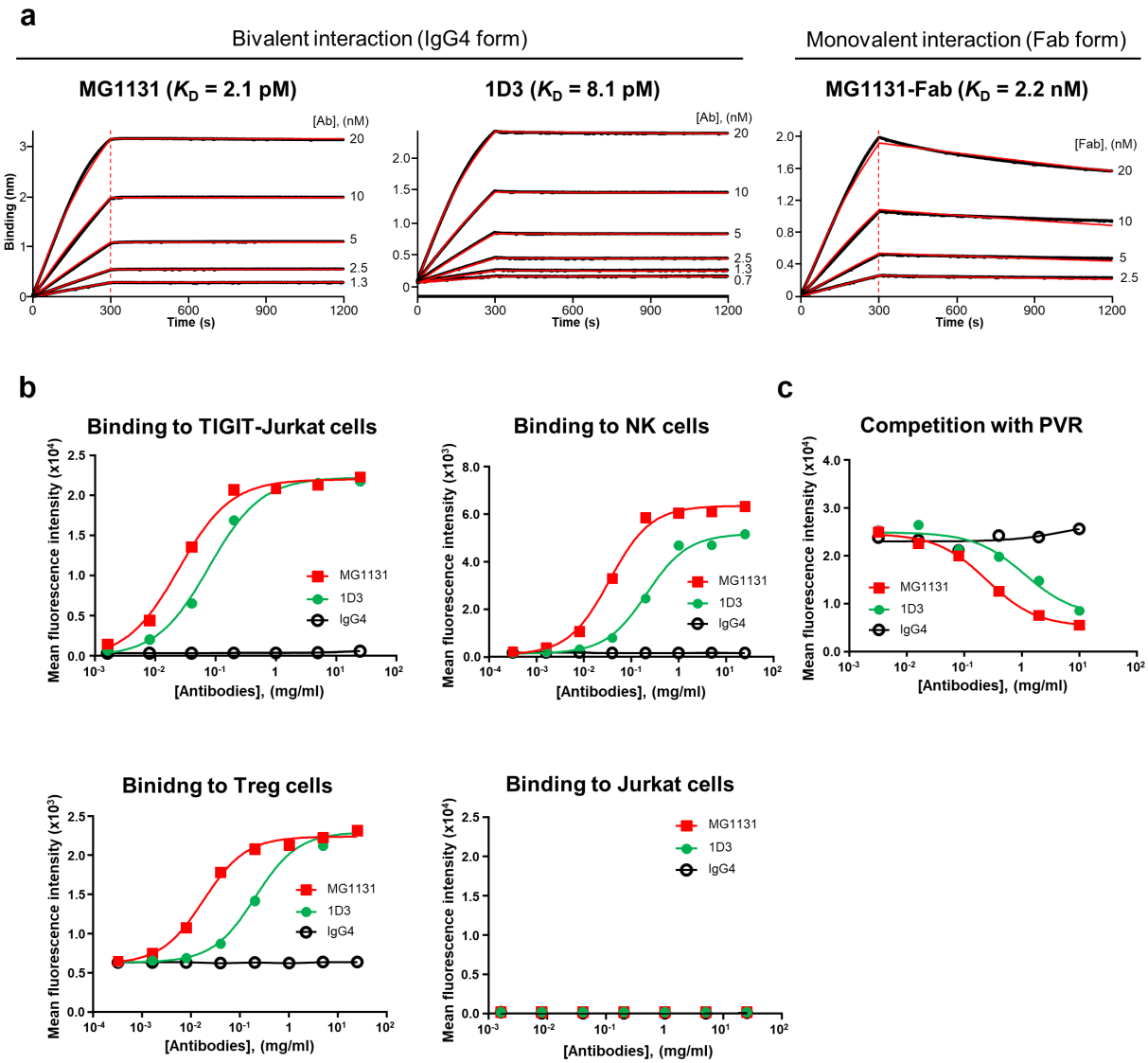

Figure 2. MG1131 binds to hTIGIT and outcompetes PVR. (A) Quantification of binding affinity by BLI. MG1131 and 1D3, both in the IgG4 form, at the indicated concentrations were reacted with hTIGIT(22–141) immobilized on a biosensor tip (*Left, Middle*). The same BLI experiment was performed for MG1131 in the Fab form (*Right*). Shown are the K_D values calculated by curve fittings (red lines) of the association and dissociation kinetics (black lines).(B) MG1131 binds to the indicated cell lines, as does 1D3. Both MG1131 and 1D3 do not exhibit detectable binding to Jurkat cells, which do not express TIGIT. The NK cells were expanded from human PBMCs, and the Treg cells were isolated from human PBMCs. Cell-bound MG1131 and 1D3 were detected by flow cytometry.(C) Competition assay. MG1131 was challenged against PVR pre-bound to hTIGIT-Jurkat cells. Cell-bound PVR was detected by flow cytometry. In *B* to *E*, representative data are shown from two independent experiments. In *B* to *E*, 1D3 was used as a reference for potency comparison, and human IgG4 as a negative control.Figure 2a Alt text: The binding affinities of MG1131 and 1D3 for hTIGIT were measured and the binding kinetics curves are shown on the left and middle panels. MG1131 binds hTIGIT more tightly than 1D3, a reference antibody developed by a company. The right panel shows the binding kinetics curves used for measuring the binding affinity of the Fab form of MG1131 for hTIGIT. Figure 2b Alt text: MG1131 and ID3 were tested for their binding to four different cells expressing hTIGIT, and their binding signals were plotted as a function of their concentration (in four panels).Figure 2c Alt text: MG1131 and ID3 were tested for their potency in competing with PVR for binding to hTIGIT-expressing cells. Reduction of PVR binding to the cell is plotted as a function of the concentration of the two proteins. In all these assays, MG1131 was better than or at least comparable to 1D3.

Table 2. X-ray data collection and structure refinement statistics.

Data Collection	MG1131-scFv—hTIGIT(23–128)
Space group	$P2_1$
Unit cell dimensions	
a, b, c (Å)	69.67, 79.82. 77.97
α, β, γ (°)	90.0, 100.55, 90.0
Wavelength (Å)	0.97957
Resolution (Å)	28.98–1.53 (1.585–1.53)[a]
R-merge	0.065 (1.283)[a]
I/σ(I)	16.00 (1.47)[a]
Completeness (%, > −3σ)	99.94 (99.93)[a]
Redundancy	7.0
Refinement	
No. of reflections	126,310 (12,548)[a]
Rwork/Rfree (%)	20.1/22.8
R.m.s deviations	
Bond (Å)/Angle (°)	0.012/1.19
Average B-values (Å^2)	25.80
Ramachandran plot (%)	
Favored/Additional allowed	98.64/1.36
Outliers	0.0

[a]The numbers in parentheses are the statistics from the highest resolution shell.

Table 3. The paratope and epitope in the MG1131-scFv–hTIGIT structure.

MG1131		hTIGIT
CDR	Paratope residues	Epitope residues
H1	Tyr^{H53}	Gln56, Asn58, Glu60, Asp63, Leu66, Ile68, Asn70, Asp72, Leu73, His76, His111, Tyr113, Thr117
H2	Ile^{H50}, Ser^{H56}, Ser^{H58}, Gln^{H61}	
H3	Trp^{H100}, Phe^{H100A}	
L1	Gln,^{L27} Ser,^{L29} Ser,^{L30} Ser,^{L31} Tyr^{L32}	
L2	None	
L3	Tyr^{L91}, Ser^{L93}, Ser^{L94}, Pro^{L95}	

Structural analyses of MG1131-scFv–hTIGIT(23-128)

We constructed an scFv version of MG1131 by connecting the variable domains of the heavy and the light chains together with a $(Gly_4Ser)_4$ linker. The complex between MG1131-scFv and hTIGIT(23–128) was crystallized and its crystal structure was determined (Table 2). The crystal contained two MG1131-scFv–hTIGIT(23–128) complexes in the asymmetric unit. No significant conformational differences were found between the two copies. Although MG1131-scFv is a single polypeptide, the structure has two chains labeled H and L, as we followed the Kabat numbering scheme of the heavy and light chains of an IgG antibody by using the abYsis annotation tool.[26,27] MG1131-scFv sits on one side of the beta-sandwich of hTIGIT(23–128) (Figure 3a), and buries the solvent-accessible surface area of 1676 Å^2 according to the PISA program.[28]

The high-resolution structure of the complex reveals detailed views of the intermolecular interactions. All of the paratope residues of MG1131-scFv, defined here as those within 4.5 Å of hTIGIT(23–128), belong to the complementarity-determining regions (CDRs) of the heavy and light chains (CDRH1-CDRH3 and CDRL1-CDRL3) (Figure 3b, Table 3). On the other hand, the epitope residues of hTIGIT are on β-strands (β5, β6, β8, β10 and β11) and on two loops (β5-β6 and β6-β7) (Figure 3b, Table 3). Of the paratope residues, Trp^{H100} (on CDRH3) appears as a key residue; its side chain is inserted into a pocket composed of the side chains of five hTIGIT epitope residues (I68, L73 Q56, N70, H76), while the ring –NH of Trp^{H100} interacts indirectly with hTIGIT (carbonyl oxygen of W75) via a water molecule (Figure 3c). Other notable paratope residues are Tyr^{L32} (on CDRL1) and Gly^{L92} (on CDRL3), which make a hydrogen-bonded network with Q56, N58, and E60 of hTIGIT (Figure 3c). This network is partly covered by the hydrophobic interactions between L65 and I68 of hTIGIT and Phe^{H100A} and Trp^{H100} of MG1131-scFv (on CDRH3).

To ensure that the MG1131-scFv–hTIGIT(23–128) crystal structure reflects the actual binding interaction between the two proteins, we introduced alanine substitution of Trp^{H100}, whose side chain is involved in extensive interaction with hTIGIT (Figure 3c). The resulting mutant, MG1131-scFv ($W^{H100}A$), exhibited virtually no detectable binding affinity (Figure 3d), demonstrating that the crystal structure is biochemically relevant.

Structural basis for blocking TIGIT by MG1131

The crystal structure of the D1 domain of PVR (residues 1–143) in complex with hTIGIT (residues 23–128) revealed that the PVR(1–143) forms a homodimer, and both monomers interact with hTIGIT(23–128), resulting in a bivalent interaction.[12] A structural comparison between MG1131-scFv–hTIGIT(23–128) and PVR(1-143)-hTIGIT(23–128) (PDB: 3UDW) shows that MG1131 binds to a surface of hTIGIT(23–128) that partly overlaps with the PVR(1-143)-binding interface on hTIGIT (Figure 3e). Especially, MG1131, via CDRH1-CDRH3 and CDRL3, interacts extensively with the conserved AX_6G motif (Ala67 to Gly74) of TIGIT, which makes a lock-and-key interaction with a conserved T(F/Y)P motif of PVR.[12] The binding affinity (in terms of K_D) between PVR and TIGIT was reported as 3.15 nM,[1] which is weaker than that between MG1131 and hTIGIT (K_D of 0.59 nM). These results are in line with the competition assay (Figure 2c) and indicate that MG1131 would be able to block PVR binding to hTIGIT, thereby inhibiting the immunosuppressive signaling of TIGIT *in vivo*. Although the structure of 1D3 bound to hTIGIT is unavailable, a patent (WO2017/053748A2) lists the epitope residues interacting with 1D3. Mapping these residues together with the MG1131 epitope residues on the hTIGIT structure reveals that, while the hTIGIT-binding orientations of MG1131 and 1D3 are apparently different from each other, the two epitope surfaces partly overlap, with six epitope residues shared by the two mAbs (figure 3f). The comparison shows that 1D3 epitope surface also partly overlaps with the PVR(1-143)-binding site on hTIGIT, suggesting a similarity in the modes of action of the two mAbs. Consistently, *in vitro* and *in vivo* experiments showed that MG1131 potently suppresses TIGIT signaling, as described below.

Effects of MG1131 on the activities of NK cells and Treg cells

Engagement of PVR on target cells with TIGIT on NK cells contributes to the suppression of immunological activities of the effector cells.[29] TIGIT is also known to be highly expressed on Treg cells and contributes to their immunosuppressive functions on the antitumor activities of effector T cells.[30–32]

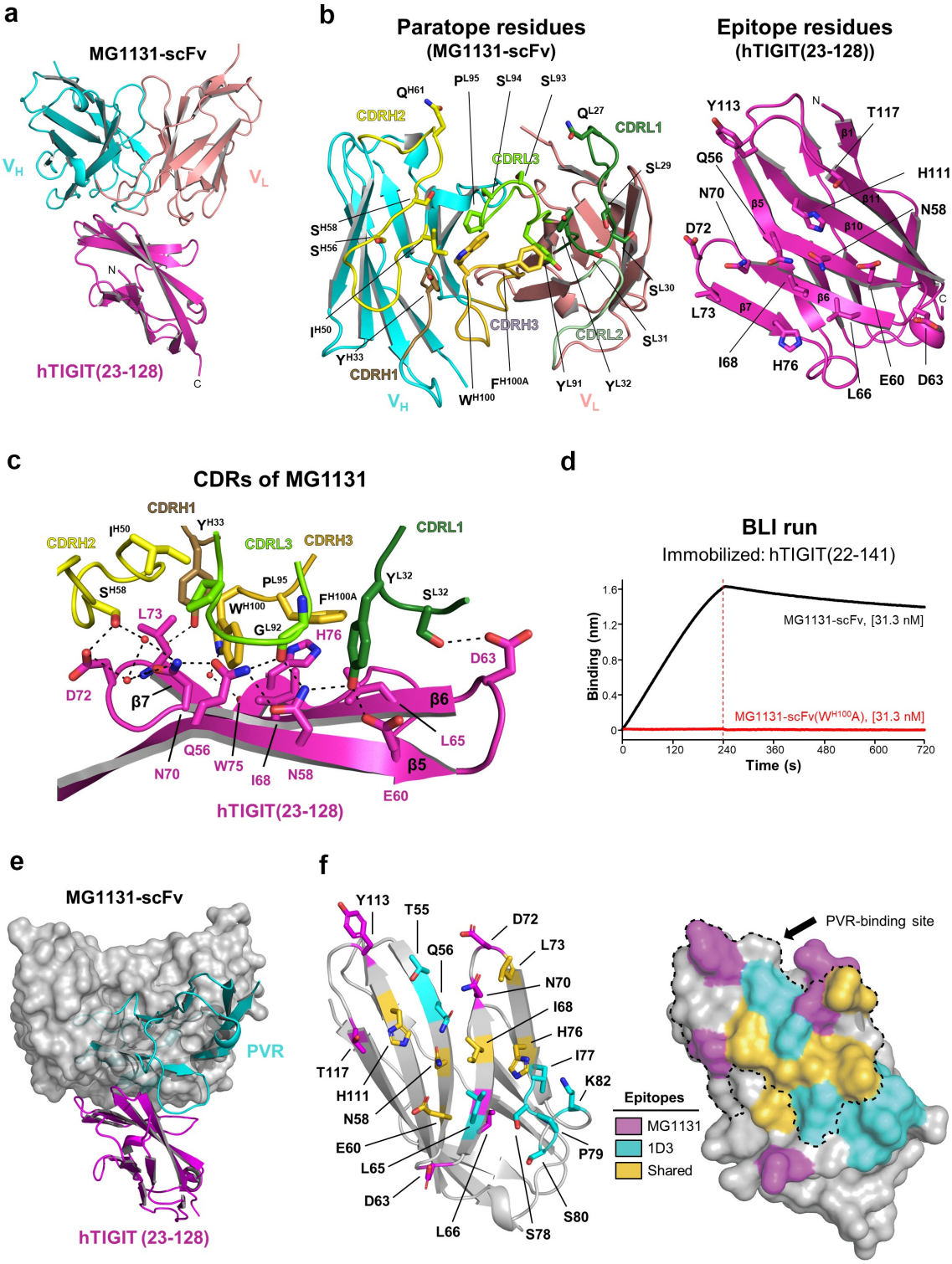

Figure 3. Interaction of MG1131-scFV with hTIGIT(23–128). (A) Crystal structure of the MG1131–scFV-hTIGIT(23–128) complex. MG1131-scFv interacts with a tip side of the elongated structure of hTIGIT(23–128) by sitting on one side of the β-sandwich.(B) The paratope and epitope residues are shown in sticks and labeled (tabulated in Table 3). The CDRs are color-coded and labeled.(C) Key paratope–epitope interactions. Residues involved in the interactions are shown in sticks. The dotted lines indicate hydrogen bonds.(D) W^{H100} is a critical paratope residue. BLI kinetics curves are shown for MG1131-scFv (31.3 nM) and MG1131-scFv(W^{H100}A) that reacted with hTIGIT(22–141) immobilized on a biosensor chip. Unlike wild-type MG1131-scFv, the mutant protein exhibited undetectable binding response at 31.3 nM.(E) MG1131-scFv and PVR(1–143) bind to an overlapping surface on hTIGIT. The structures of MG1131-scFv–hTIGIT(23–128) and PVR(1–143)–hTIGIT(23–128) (PDB: 3UDW) were superposed by aligning the common hTIGIT(23–128) molecule in the two structures. MG1131-scFv in surface representation overlaps severely with PVR (1–143) in ribbon representation due to a partial overlap of the binding surfaces on TIGIT.(F) Epitope ComparisonFigure 3a Alt text: Crystal structure of the scFv form of MG1131 bound to hTIGIT is shown to illustrate the binding interaction between the antibody and the antigen.Figure 3b Alt text: (Left) Paratope residues of MG1131, which are involved in binding to hTIGIT, are shown in stick and labeled. (Right) Epitope residues of hTIGIT, which are involved in binding to MG1131, are shown in sticks and labeled.Figure 3c Alt text: Key interactions between MG1131 and hTIGIT are shown in a magnified view. Of these, the tryptophan residue at the 100th residue position is outstanding.Figure 3d Alt text: A binding curve shows that the alanine substitution of this tryptophan residue drastically reduced the binding affinity for hTIGIT. Figure 3e Alt text: Structural superposition shows that MG1131-binding site overlaps with the PVR-binding site on the surface of hTIGIT.figure 3f Alt text: Mapping of the epitope residues of MG1131 and 1D3 on the crystal structure of hTIGIT shown in stick representation (left) and in surface representation (right). The two antibodies share six epitope residues.

We first investigated whether MG1131 would affect the cytotoxicity of NK cells against PVR-positive target cells: a Raji stable cell line expressing PVR-GFP (PVR-GFP-Raji) and H358 cells. Upon treatment of these cells with MG1131, the cytotoxicity of the NK cells was enhanced in a dose-dependent manner and in a PVR-dependent manner (Figure 4a). Next, we evaluated the effect of MG1131 on the suppressive function of Treg cells by monitoring the proliferation of $CD8^+$ T cells in total PBMCs co-cultured with Treg cells. Indeed, MG1131 treatment decreased expression of inhibitory immune checkpoint molecules, including CTLA-4, CD39, and PD-1 on Treg cells (Figure 4b). Consistently, the treatment significantly decreased the suppressive activity of Treg cells (Figure 4c). These data demonstrate that MG1131 enhances NK cell-mediated killing of cancer cells and downregulates the immunosuppressive functions of Treg cells.

Effects of MG1131 on PBMCs from multiple myeloma patients

During the progression of multiple myeloma, $CD8^+$ T cells exhibit increased expression of TIGIT and these TIGIT-positive $CD8^+$ T cells exhibit impaired cytotoxicity.[22] It was shown that TIGIT blockade by a mAb improved the cytotoxic activities of $CD8^+$ T cells obtained from multiple myeloma patients.[22] To examine whether MG1131 exerts similar effects, PBMCs from multiple myeloma patients were stimulated with anti-CD3/CD28 microbeads and incubated with MG1131. Measurement of the secreted interferon (IFN)-γ level indeed demonstrated that MG1131 significantly enhanced IFN-γ production by the PBMCs, presumably owing to restored cytotoxic functions of $CD8^+$ T cells (Figure 4d). This result suggests that MG1131 could promote T cell immunity against multiple myeloma.

Antitumor efficacy of MG1131 in transgenic mouse models

Since human TIGIT cross-reacts with mouse PVR,[33] and since MG1131 does not cross-react with mouse TIGIT (data not shown), the *in vivo* efficacy of MG1131 was evaluated using the TIGIT HuGEMM mice, which were genetically engineered to express a chimeric human/mouse TIGIT protein with the extracellular domain of human TIGIT and the transmembrane and intracellular domains of mouse TIGIT. The mice successfully engrafted with the Hepa 1–6 tumor cells were randomly divided into treatment groups, and 10 mg/kg of MG1131 or phosphate-buffered saline (PBS) was administered twice per week. MG1131 exhibited 58% tumor growth inhibition (TGI) with increased infiltration of $CD3^+$ T cells into the tumor (Figure 5a). The antitumor efficacy of MG1131 was further evaluated in a mouse xenograft tumor model using the immunodeficient NOG mice in which human immune cells can be reconstituted. NOG mice were injected with HT29 cell (human colorectal adenocarcinoma cell line) and reconstituted with human PBMCs. Administration of MG1131 to NOG mice engrafted with HT29 cells resulted in 28% TGI (Figure 5b). The reduction of the tumor volume in the treatment group in comparison with the control group is significant, but not striking. We speculate that this modest efficacy is due to development of xenograft-versus-host disease (xGvHD), which is the primary drawback of human PBMC engraftment into the mouse.[34] Initially, upon infusion of 10 ~ $15x10^6$ human PBMCs into the mouse, we observed severe effects of the xGvHD in a few weeks. We therefore reduced the number to $7x10^6$, which might not have been sufficient for inducing maximum efficacy. Moreover, the influences of the xGvHD and the graft-versus-tumor reactivity may lead to slow growth of the engrafted tumor, which was at day 15 to 18 in our case, resulting in less pronounced differences of tumor growth inhibition between the two groups, as similarly observed by others.[35] These data together with the results from the *in vitro* study suggest that MG1131 is a promising candidate for cancer immunotherapy.

Discussion

The extracellular domain of TIGIT is relatively small (with a single Ig variable domain), and notably contains many exposed hydrophobic residues (Leu65, Ile68, Leu73, Phe107, Ile109, Pro124, Phe123) on one face of the β-sandwich, which is a part of the binding interface for PVR. Likely, antibodies discovered by using TIGIT as bait would interact with some of these residues, and thus compete with PVR for binding to TIGIT. Consistently, all of the 11 positive clones found in the phage display library of scFvs exhibited competitive binding to TIGIT in the presence of PVR, suggesting the relative ease of finding an array of anti-TIGIT antibodies with a varying binding mode and binding affinity. To our knowledge, the reported structure is the first structure of an antibody or antibody fragment bound to TIGIT, although many preclinical or clinical trials involving an anti-TIGIT mAb are currently underway. It is hard to predict whether a mAb, with its bivalent binding mode, would promote or disrupt homodimerization of TIGIT in *cis*, which is known to be a weak interaction, but critical for signaling. Additional reports on structures and properties of other anti-TIGIT mAbs may pave the way to suppress TIGIT for potent antitumor efficacy and successful clinical application.

We deliberately constructed MG1131 as the IgG4 type, rather than the IgG1 type, to avoid potential depletion of antitumor effector cells, such as T cells and NK cells, owing to the reduced binding of the IgG4 Fc to Fc-gamma receptors (FcγRs) (in comparison with the IgG1 Fc) and thus to the reduced induction of effector functions of the Fc.[36] However, another possibility is that IgG1-type mAb might be advantageous, since it may remove Treg cells from tumor microenvironment by invoking antibody-dependent cellular cytotoxicity via the Fc, although it accompanies the risk of damaging antitumor effector cells simultaneously. So far, the question of whether the Fc-FcγR engagement is required for the full therapeutic efficacy of TIGIT mAb has not clearly been answered.[37] Further studies that directly compare the antitumor efficacy of mAbs of different IgG types, but with the same Fab, are needed. Considering the enhanced antitumor activity of chimeric antigen receptor-T cells (CAR-T cells) upon blocking immune checkpoint inhibition by an anti-PD-1 or anti-PD-L1 antibody,[38–40] adoptive cell therapy could benefit from incorporating an anti-TIGIT mAb. In this combination, the IgG4-type might be advantageous, since the IgG1-type mAb could damage CAR-T cells by the effector functions of its Fc.

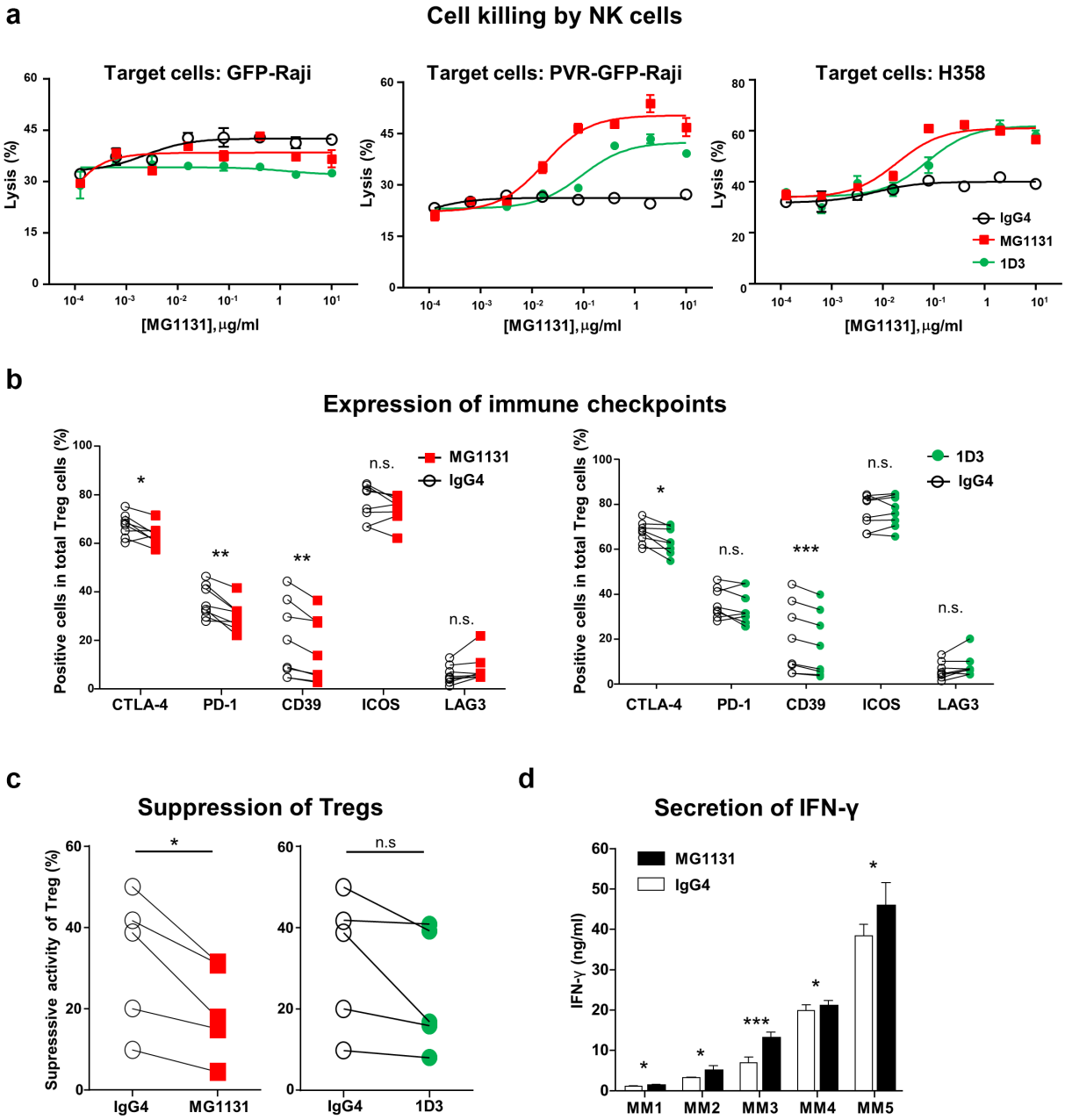

Figure 4. Antitumor activity of MG1131 in cell-based assays. (A) Increased cytotoxic activity of NK cells. Expanded NK cells were co-cultured with the indicated target cells (stained with calcein AM) with an E:T ratio of 10:1, and the levels of fluorescence from the supernatant were measured as a function of the concentration of MG1131 or 1D3. N = 3. Bars: mean ± standard error of the mean. (B) Decreased expression of immune checkpoint proteins. Following T cell activation, Treg cells were treated with MG1131 or 1D3 at 10 μg/mL. The expression of the indicated immune checkpoint proteins on Treg cells was detected by flow cytometry. Treg cells were $CD3^{+}CD4^{+}CD25^{hi}CD127^{lo}FoxP3^{+}$ cells. Treg cells from nine different donors were used. *, $p < .05$; **, $p < .01$ by paired t-test. In A-C, human IgG4 was used as a control. (C) Decreased activity of Treg cells. CFSE-labeled Tresp cells were activated with anti-CD3/CD28 microbeads, treated with MG1131 or 1D3 at 10 μg/mL, and cultured with or without Treg cells for 5 days. The suppressive activity of Treg cells was calculated based on the proliferation of Tresp cells (see Materials and Methods). Five pairs of the marks (○, ■) represent five different donors. $p < .05$ by paired t-test.(D) Improved cytotoxic activities of $CD8^{+}$ T cells derived from multiple myeloma patients. Following T cell activation with anti-CD3/CD28 microbeads, PBMCs from multiple myeloma patients were incubated with MG1131 or human IgG4 (control) at 10 μg/mL for 4 days. Secretion of IFN-γ was measured by flow cytometry. Results from five different donors (MM1-MM5) are shown. Bars: mean ± SEM. *, $p < .05$, ***, $p < .005$ by unpaired t-test.Figure 4a Alt text: The effect of MG1131 and 1D3 on the cell killing activity of natural killer cells were measured for three different cell lines. Line graphs show the increase in the cytotoxicity activity of natural killer cells as a function of the concentration of the two antibodies.Figure 4b Alt text: The effects of MG1131 and 1D3 on the expression of immune checkpoint proteins are shown on the left and right panel, respectively. The two antibodies decrease the expression of these proteins. Figure 4c Alt text: The effects of MG1131 and 1D3 on the suppression of regulatory T cells are shown on the left and right panel, respectively. In these experiments (in Figure 4a-4c), MG1131 was better than or at least comparable to 1D3.Figure 4d Alt text: A bar graph showing the secretion of IFN-γ in PBMCs derived from multiple myeloma patients. MG1131 treatment enhanced the IFN-γ secretion in comparison with the control IgG4 antibody.

In conclusion, we developed MG1131, a high-affinity IgG4-type mAb against hTIGIT. It exhibits antitumor activities *in vitro* and *in vivo*, which is likely to arise at least from blocking the interactions between TIGIT and its cellular binding partners. Combined with another immune checkpoint inhibitor, such as anti-PD-1 mAb, or with CAR-T cells, MG1131 may be further developed into a cancer immunotherapy biologic.

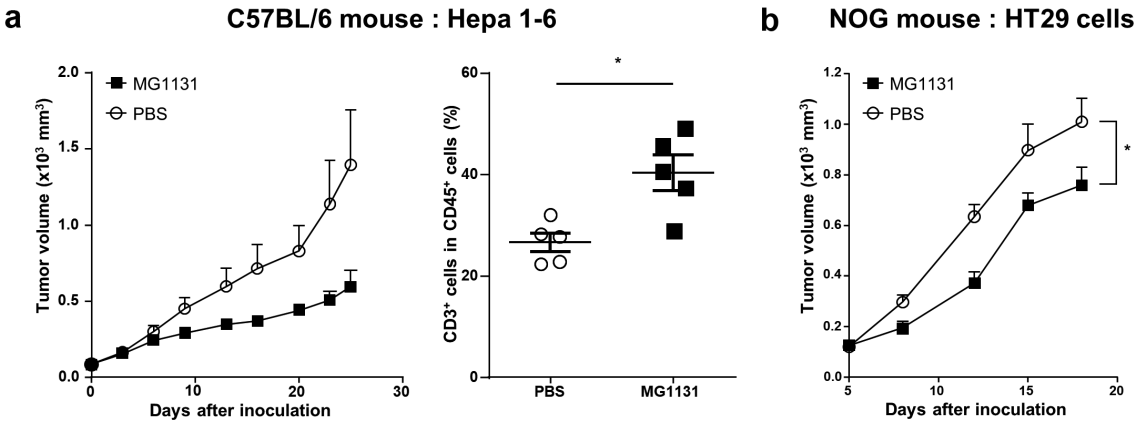

Figure 5. Antitumor efficacy of MG1131 in mouse tumor models. (A) Hepa1-6 cell-derived xenograft was established in C57BL/6 mice that were engineered to express hTIGIT. At day 5, MG1131 or PBS was administered intraperitoneally at 10 mg/kg twice per week. Time-course tumor volume (*Left*) and % of $CD3^+$ T cells in TILs at day 18 (*Right*) are shown. N = 5. **, $p < .05$ by unpaired t-test.(B) NOG mice were implanted with HT29 cells subcutaneously and injected with healthy donor PBMCs intraperitoneally on day 0. At day 5, MG1131 or PBS was administered intraperitoneally at 10 mg/kg three times per week. Time-course tumor volume is shown. N = 8 (MG1131) or 12 (PBS). *, $p < .05$ by unpaired t-test on day 18.Figure 5a Alt text: (Left) MG1131 suppressed tumor growth in Hepa1-6 cell-based xenograft mice, which was traced in a time course manner. PBS buffer was used as a control. (Right) Furthermore, MG1131-treated mice showed more CD3-positive cells in tumor-infiltrating lymphocytes compared with PBS buffer-treated mice.Figure 5b Alt text: Time course measurement of tumor volume is shown, which was measured for NOG mice implanted with HT29 tumor cells. MG1131 treatment retarded the tumor growth considerably in comparison with PBS buffer treatment.

Materials and methods

Discovery of anti-hTIGIT antibodies

hTIGIT-His (Creative biomart) was used as bait to screen a naïve human scFv phage library (Myxengo) to identify 11 clones, which were converted into IgG1-type mAbs. The binding affinity of these mAbs for hTIGIT was analyzed by the enzyme-linked immunosorbent assay (ELISA) on a plate coated with on hTIGIT-Fc (R&D systems, Cat # 7898_TG) as previously described.[41]

Expression and purification of MG1131 and a reference antibody 1D3

Codon-optimized DNA fragments encoding the heavy and the light chain of MG1131 or tiragolumab were each cloned into the pCIW2 vector (GC Pharma) or the pMSID2 vector (GC Pharma), respectively, to construct IgG4-type mAb. This in-house version of tiragolumab, named 1D3, was used as a reference mAb. MG1131 and 1D3 were produced by using CHO DG44 cells (originated from Dr. Lawrence Chasin at Columbia University) and ExpiCHO Expression System Kit (Thermo Fisher Scientific), respectively. For both mAbs, harvested cell culture fluid was loaded onto an XK 50/20 column packed with MabSelect SuRe resin (Cytiva). The column was washed with 5 column volumes (CVs) of the PBS buffer (pH 7.0), and bound 1D3 or MG1131 was eluted with 0.1 M glycine buffer (pH 3.0 ~ 3.2), titrated to pH 5.5 by adding 1 M Tris, dialyzed against the PBS buffer and filtered through a 0.22 μm filter.

Binding affinity measurement by biolayer interferometry (BLI)

BLI experiments were performed using an Octet R8 protein analysis system (Sartorius). Each well contained 200 μL of solution, and the assay buffer was the Kinetics Buffer (Satorius, PBS+ 0.02% Tween20, 0.1% BSA, 0.05% sodium azide). Streptavidin biosensor tips (Sartorius) were loaded with biotinylated hTIGIT(22–141) (Acrobio Systems) at 2 ng/μL for 120 s (threshold of 1.5 nm response), incubated in the Kinetics Buffer for 60 s to acquire the baseline measurement, dipped into the solution containing the analyte for 300 s (association step) and dipped into the same buffer for 900 s (dissociation step). The kinetics data were analyzed with the Octet BLI Analysis 12.2 software package (Sartorius).

Generation of stable cell lines

To generate a TIGIT-expressing stable Jurkat cell line (hTIGIT-Jurkat), full-length hTIGIT cDNA (Origene) was cloned into the pEF1α-AcGFP-N1 vector (Clontech), and the plasmid was introduced into Jurkat E6.1 cells (ATCC). GFP-positive Jurkat cells were sorted out using a FACSAria II (BD). PVR-GFP-Raji and control stable Raji cells expressing GFP (GFP-Raji) were generated similarly by using full-length human PVR cDNA (Dharmacon) and Raji cells (ATCC).

Isolation of Treg cells and expansion of NK cells from human PBMCs

Leukapheresis products were collected from healthy donors at Samsung Medical Center (institutional review board: No. 2018–01-089) and PBMCs were isolated by centrifugation on a Ficoll density gradient (GE Healthcare). Treg cells were isolated from the human PBMCs using the EasySep™ Human $CD4^+CD127^{low}CD25^+$ Regulatory T cell isolation kit (STEMCELL Technologies). The purity of isolated Treg cells ($CD4^+CD127^-CD25^+FoxP3^+$ cells) was determined by flow cytometry using the fluorochrome-conjugated antibodies (Table 4) and an LSRFortessa instrument (BD). Intracellular staining was performed using the FoxP3/Transcription Factor Staining Buffer (eBioscience). For NK cell expansion, human PBMCs were cultured in the CellGro SCGM (CellGenix) supplemented with 10 ng/mL OKT3 (anti-CD3 mAb; eBioscience),

500 IU/mL IL-2 (Novartis) and 5% human plasma (Valley Biomedical) in a culture bag (NIPRO). Fresh culture medium was added every 2–3 days to reach the cell density of 1×10^6 cells/mL.

Cell-based antibody-binding assay

The hTIGIT-Jurkat cells (3×10^5 cells/well), the isolated Treg cells (1×10^5 cells/well), or the expanded NK cells (2×10^5 cells/well) on a 96-well round-bottom plate were treated with the anti-TIGIT mAbs including MG1131 at varying concentration and incubated for 90 min. Antibodies bound to the hTIGIT were detected with the anti-Human IgG $F(ab')_2$ Fragment-R-Phycoerythrin antibody (Sigma Aldrich, Cat # P8047) by flow cytometry. The IC_{50} values were determined by analyzing the mean fluorescence intensity (MFI).

Ligand competition assay

The hTIGIT-Jurkat cells (2×10^5 cells/well) on a 96-well round-bottom plate were treated with 50 μg/mL of human PVR-Fc and incubated for 1 h. Cells were washed and treated with the varying concentration of anti-TIGIT mAbs or control human IgG4 (Sigma Aldrich, Cat # I4639). Cells were incubated for 90 min, stained with phycoerythrin (PE)-conjugated anti-human PVR antibody (R&D systems, Cat # FAB25301P), washed and analyzed by flow cytometry. The IC_{50} values were determined by analyzing the MFI.

Luciferase reporter assay in Jurkat cells

The assay was performed using the TIGIT/CD155 Blockade Bioassay (Promega) according to the manufacturer's instructions, and the luminescence intensity was measured using a GloMax Discover microplate reader (Promega).

In vitro cytotoxicity assay

On day 21 post expansion, NK cells as the effector cells were seeded (1×10^5 cells/well) and pre-incubated with varying concentration of MG1131 or human IgG4 (Sigma Aldrich). Calcein AM (Invitrogen)-stained GFP-Raji, GFP-PVR-Raji or H358 cells (ATCC) as the target cells were added at the Effector:Target (E:T) ratio of 10:1. 100 μL of the supernatant was transferred to a black 96-well flat-bottom plate and fluorescence intensity was measured using a VICTOR X3 plate reader (PerkinElmer) (485 nm/535 nm, 0.1 s). The percentage of target cell lysis was calculated using the formula, Lysis % = [(Test release–Spontaneous release)/(Maximum release+(Assay media release–2% Triton X-100 release)–Spontaneous release)] x 100.

Table 4. Fluorochrome-conjugated antibodies used for flow cytometry analyses.

Species reactivity	Antibody	Clone	Fluorochrome	Supplier
Human	CD3	SK7	APC-H7	BD
	CD4	RPA-T4	APC-R700	BD
	CD25	M-A251	BV421	BD
	CD127	HIL-7RM21	BB515	BD
	FoxP3	PCH101	PE	eBioscience
	CD39	eBioA1	PE-Cy7	eBioscience
	PD-1	EH12.2H7	PE-Cy7	Biolegend
	ICOS	C398.4A	Alexa647	Biolegend
	LAG3	11 C3C65	PE-Cy7	Biolegend
	CTLA-4	polyclonal	APC	R&D systems
Mouse	CD45	30-F11	PerCP-Cy5.5	Biolegend
	CD3	17A2	BUV395	BD
-	Fixable viability dye	-	eFluo780, V500	Invitrogen

Immunophenotypic analysis of Treg cells

The human PBMCs (1×10^6 cells/well) on a 96-well round-bottom plate were stimulated with Dynabeads Human T-Activator CD3/CD28 (Gibco) in the presence of 10 μg/ml of MG1131 or control human IgG4 for 6 days. Cells were stained with the fluorochrome-conjugated antibodies (Table 4). Intracellular staining was performed using the FoxP3/Transcription Factor Staining Buffer (eBioscience). The expression of the immune checkpoint proteins on Treg cells ($CD3^+CD4^+CD25^{hi}CD127^{low}FoxP3^+$) was analyzed by flow cytometry.

In vitro assay for the suppression of PBMCs by Treg cells

Treg cells isolated from human PBMCs were used as effector cells and autologous total PBMCs were used as responder cells (Tresp cells). CFSE (Invitrogen)-labeled total PBMCs were seeded at 2×10^5 cells/well, and Treg cells were added at a Treg:Tresp ratio of 0.25:1 (or 0:1 for the control). Cells were stimulated with 2 μg/ml of anti-CD3 mAb (eBioscience, Cat # 16–0037-85) and anti-CD28 mAb (eBioscience, Cat # 16–0289-81) for T cell activation in the presence of 10 μg/ml of MG1131 or control human IgG4 for 5 days. The proliferation of Tresp cells was analyzed by assessing the percentage of $CFSE^{lo}$ dividing cells within the $CD3^+CD8^+$ cells by flow cytometry. The percentage of suppression was calculated according to the formula, [100-(% proliferated Tresp+% proliferated Treg)/% proliferated Tresp] x 100.

Measurement of IFN-γ secretion from multiple myeloma patient-derived PBMCs

PBMCs from multiple myeloma patients (Axol and iQ Bioscience) were thawed and seeded at 1×10^6 cells/well. Cells were treated with Dynabeads Human T-Activator CD3/CD28 (Gibco) for activation of T cells in the presence of 10 μg/ml of MG1131 or control human IgG4 for 4 days. The levels of IFN-γ in the culture supernatant were analyzed by flow cytometry using a CBA Human Th1/Th2/Th17 Cytokine Kit (BD).

Evaluation of the antitumor efficacy of MG1131 in the TIGIT HuGEMM mice

Each TIGIT HuGEMM mouse (background: C57BL/6; generated by Crown Bio) was inoculated subcutaneously at the right flank region with 5×10^6 Hepa 1–6 tumor cells in 0.1 mL of PBS. When the mean tumor volume

reached approximately 100 mm^3, mice were randomly selected into treatment groups and treated with MG1131 (10 mg/kg) or PBS by intraperitoneal injection twice per week. Mean TGI was calculated according to the formula, TGI % = (1–Ti/Ci) x 100, where Ti and Ci are the mean tumor volume of the treatment group and the control group, respectively, on the same measurement day. TILs were isolated by using the Tumor Dissociation Kit (Miltenyi Biotec) and gentleMACS Octo Dissociator (Miltenyi Biotec). Cells were treated with Mouse Fc Block (BD, Cat # 553141), stained with the fluorochrome-conjugated antibodies (Table 4) and analyzed by flow cytometry. All of the *in vivo* analyses using the TIGIT HuGEMM mice were conducted at the Crown Bio.

Evaluation of the antitumor efficacy in an HT29 xenograft mouse model

Six-week-old female NOG mice (NOD.Cg-Prkdc^{scid}Il2rg^{tm1Sug}/Jic) were subcutaneously inoculated with 3.5×10^6 HT29 cells in 0.2 mL of PBS at a right flank region on day 0. After 3–4 h, 7×10^6 human PBMCs in 0.2 mL of PBS were injected intraperitoneally to reconstitute a human immune system. When the mean tumor volume reached approximately 100 mm^3, mice were randomized into treatment groups and treated with MG1131 (10 mg/kg) or PBS by intraperitoneal injection three times per week. Tumor volume and TGI were calculated (IACUC of the GC Pharma: No. GC-18-008A).

Expression and purification of MG1131-scFv and hTIGIT (23-128)

To produce MG1131-scFv, $(Gly_4Ser)_4$ linker was inserted between the variable regions of heavy and light chains in the form of DNA by standard polymerase chain reaction. The DNA fragment was cloned into a modified version of the pET 22b vector (Novagen) and expressed with a C-terminally fused cysteine protease domain (CPD) of *vibrio cholerae* MARTX toxin with a $(His)_{10}$ tag from *E. coli* BL21 (DE3) RIPL strain (Agilent). Cells were grown at 18°C after 250 µM isopropyl β-D-1-thiogalactopyranoside (IPTG) induction. Bacterial cell lysates were prepared by sonication in buffer A (20 mM Tris-HCl, pH 7.5 and 150 mM NaCl). The supernatant was applied to a HisPur™ Ni-NTA resin (Thermo Fisher Scientific). The CPD-$(His)_{10}$ tag was cleaved autolytically on gel by adding 100 µM sodium phytate (Sigma Aldrich). The unbounded fraction was further purified using a Hitrap Q anion exchange column (Cytiva) and a HiLoad 26/60 Superdex 75 gel-filtration column (Cytiva). A fragment of hTIGIT encompassing residues 23–128, designated as hTIGIT(23–128), was produced and purified by the procedures that are virtually identical to those used for MG1131-scFv, except for using the *E.coli* Rosetta-gami 2 (DE3) strain (Novagen).

Crystallization and structure determination of MG1131-scFv–hTIGIT(23-128)

Purified MG1131-scFv and hTIGIT(23–128) were mixed together in an 1:1.2 molar ratio and then loaded onto a HiLoad 26/60 Superdex 75 gel-filtration column (Cytiva) equilibrated with buffer A. The fractions containing the MG1131-scFv-hTIGIT(23–128) complex were concentrated by using Amicon Ultra-15 Centrifugal Filter (Merck Millipore). MG1131-scFv-hTIGIT(23–128) (20 mg/mL) was crystallized in a solution composed of 200 mM ammonium citrate and 20% (v/v) polyethylene glycol 3350 at 20°C. For cryoprotection, the crystals were briefly immersed into the mother liquor containing additional 20% (v/v) ethylene glycol. X-ray diffraction data were collected at 100 K on the beamline 5 C at the Pohang Accelerator Laboratory and processed with XDS.[42] Phases were determined by the molecular replacement protocol in PHENIX using the structure of an Fv (PDB: 6EHV) and the structure of the TIGIT IgV domain (PDB: 3UCR) as search models.[43] Model building and structure refinement were performed using COOT and PHENIX.[43,44] (Table 2)

Atomic coordinates have been deposited in the Protein Data Bank under the accession code 7VYT.

List of abbreviations

CAR-T cellsChimeric antigen receptor-T cells
DNAM1DNAX accessory molecule 1
FcγRsFc-gamma receptors
IgGImmunoglobulin G
ITIMImmunoreceptor tyrosine-based inhibitory motif TIGIT
ITTImmunoglobulin tail tyrosine
mAbMonoclonal antibody
PBMCPeripheral blood mononuclear cell
PVRPoliovirus receptor
TGITumor growth inhibition
TIGITT-cell immunoglobulin and ITIM domain
xGvHDxenograft-versus-host disease

Acknowledgments

This work has been supported by the MOGAM Institute for Biomedical research and GC Pharma. The X-ray data were collected on the Beamline 5C at the Pohang Accelerator Laboratory, Korea. All figures presenting protein structures were generated using PyMOL 2.0.

Disclosure statement

H.N., J.L., H.P., J.H.S., E.S. and M.K. are co-inventors in a provisional patent application (PCT-KR2020-006705) covering the anti-hTIGIT mAb described in this article. The rest of the authors declare no competing interests.

Funding

This work was supported by the MOGAM institute for Biomedical research [MG1131A]; GC pharma [MG1131A].

ORCID

Bo-Seong Jeong http://orcid.org/0000-0003-0629-6722
Byung-Ha Oh http://orcid.org/0000-0002-6437-8470

Author contributions

B.-S.J performed protein production and structural analysis. H.N., J.L., H.-Y.P. and J.H.S. measured the activities of antibodies. K.J.C designed and constructed scFvs. E.S. performed protein-binding

assay. M.O., S.L., H.C. and J.-E.Y. produced antibodies. B.-H.O. and M.K. conceived the experiments. B.-H.O, M.K., B.-S.J., H.N. and J. L. wrote the manuscript.

References

1. Yu X, Harden K, Gonzalez LC, Francesco M, Chiang E, Irving B, Tom I, Ivelja S, Refino CJ, Clark H, et al. The surface protein TIGIT suppresses T cell activation by promoting the generation of mature immunoregulatory dendritic cells. Nat Immunol. 2009;10:48–57.
2. Stanietsky N, Simic H, Arapovic J, Toporik A, Levy O, Novik A, Levine Z, Beiman M, Dassa L, Achdout H, et al. The interaction of TIGIT with PVR and PVRL2 inhibits human NK cell cytotoxicity. Proc Natl Acad Sci U S A. 2009;106:17858–63.
3. Manieri NA, Chiang EY, Grogan JL. TIGIT: a key inhibitor of the cancer immunity cycle. Trends Immunol. 2017;38:20–28.
4. Boles KS, Vermi W, Facchetti F, Fuchs A, Wilson TJ, Diacovo TG, Cella M, Colonna M . A novel molecular interaction for the adhesion of follicular CD4 T cells to follicular DC. Eur J Immunol. 2009;39:695–703.
5. Liu S, Zhang H, Li M, Hu D, Li C, Ge B, Jin B, Fan Z . Recruitment of Grb2 and SHIP1 by the ITT-like motif of TIGIT suppresses granule polarization and cytotoxicity of NK cells. Cell Death Differ. 2013;20:456–64.
6. Dougall WC, Kurtulus S, Smyth MJ, Anderson AC. TIGIT and CD96: new checkpoint receptor targets for cancer immunotherapy. Immunol Rev. 2017;276:112–20.
7. Masson D, Jarry A, Baury B, Blanchardie P, Laboisse C, Lustenberger P, Denis MG. Overexpression of the CD155 gene in human colorectal carcinoma. Gut. 2001;49:236–40.
8. Pende D, Spaggiari GM, Marcenaro S, Martini S, Rivera P, Capobianco A, Falco M, Lanino E, Pierri I, Zambello R, et al. Analysis of the receptor-ligand interactions in the natural killer-mediated lysis of freshly isolated myeloid or lymphoblastic leukemias: evidence for the involvement of the Poliovirus receptor (CD155) and Nectin-2 (CD112). Blood. 2005;105:2066–73.
9. Carlsten M, Norell H, Bryceson YT, Poschke I, Schedvins K, Ljunggren HG, Kiessling R, Malmberg KJ. Primary human tumor cells expressing CD155 impair tumor targeting by down-regulating DNAM-1 on NK cells. J Immunol. 2009;183:4921–30.
10. Chauvin JM, Pagliano O, Fourcade J, Sun Z, Wang H, Sander C, Kirkwood JM, Chen TT, Maurer M, Korman AJ, et al. TIGIT and PD-1 impair tumor antigen-specific CD8(+) T cells in melanoma patients. J Clin Invest. 2015;125:2046–58.
11. Johnston RJ, Comps-Agrar L, Hackney J, Yu X, Huseni M, Yang Y, Park S, Javinal V, Chiu H, Irving B, et al. The immunoreceptor TIGIT regulates antitumor and antiviral CD8 (+) T cell effector function. Cancer Cell. 2014;26:923–37.
12. Stengel KF, Harden-Bowles K, Yu X, Rouge L, Yin J, Comps-Agrar L, Wiesmann C, Bazan JF, Eaton DL, Grogan JL. Structure of TIGIT immunoreceptor bound to poliovirus receptor reveals a cell-cell adhesion and signaling mechanism that requires cis-trans receptor clustering. Proc Natl Acad Sci U S A. 2012;109:5399–404.
13. Bottino C, Castriconi R, Pende D, Rivera P, Nanni M, Carnemolla B, Cantoni C, Grassi J, Marcenaro S, Reymond N, et al. Identification of PVR (CD155) and Nectin-2 (CD112) as cell surface ligands for the human DNAM-1 (CD226) activating molecule. J Exp Med. 2003;198:557–67.
14. Chan CJ, Martinet L, Gilfillan S, Souza-Fonseca-Guimaraes F, Chow MT, Town L, Ritchie DS, Colonna M, Andrews DM, Smyth MJ . The receptors CD96 and CD226 oppose each other in the regulation of natural killer cell functions. Nat Immunol. 2014;15:431–38.
15. Bowers JR, Readler JM, Sharma P, Excoffon KJDA. Poliovirus receptor: More than a simple viral receptor. Virus Res. 2017;242:1–6.
16. Shibuya A, Campbell D, Hannum C, Yssel H, FranzBacon K, McClanahan T, Kitamura T, Nicholl J, Sutherland GR, Lanier LL, et al. DNAM-1, a novel adhesion molecule involved in the cytolytic function of T lymphocytes. Immunity. 1996;4:573–81.
17. Kong YX, Zhu LL, Schell TD, Zhang JH, Claxton DF, Ehmann WC, Rybka WB, George MR, Zeng H, Zheng H . T-cell immunoglobulin and ITIM domain (TIGIT) associates with CD8(+) T-cell exhaustion and poor clinical outcome in AML patients. Clin Cancer Res. 2016;22:3057–66.
18. Han JH, Cai M, Grein J, Perera S, Wang H, Bigler M, Ueda R, Rosahl TW, Pinheiro E, LaFace D, et al. Effective anti-tumor response by TIGIT blockade associated with fcgammar engagement and myeloid cell activation. Front Immunol. 2020;11:573405.
19. Holder KA, Grant MD. TIGIT blockade: a multipronged approach to target the HIV reservoir. Front Cell Infect Microbiol. 2020;10:175.
20. Hung AL, Maxwell R, Theodros D, Belcaid Z, Mathios D, Luksik AS, Kim E, Wu A, Xia Y, Garzon-Muvdi T, et al. TIGIT and PD-1 dual checkpoint blockade enhances antitumor immunity and survival in GBM. Oncoimmunology. 2018;7:e1466769.
21. Judge SJ, Darrow MA, Thorpe SW, Gingrich AA, O'Donnell EF, Bellini AR, Sturgill IR, Vick LV, Dunai C, Stoffel KM, et al. Analysis of tumor-infiltrating NK and T cells highlights IL-15 stimulation and TIGIT blockade as a combination immunotherapy strategy for soft tissue sarcomas. J Immunother Cancer. 2020;8:e001355.
22. Guillerey C, Harjunpaa H, Carrie N, Kassem S, Teo T, Miles K, Krumeich S, Weulersse M, Cuisinier M, Stannard K, et al. TIGIT immune checkpoint blockade restores CD8(+) T-cell immunity against multiple myeloma. Blood. 2018;132:1689–94.
23. Stamm H, Oliveira-Ferrer L, Grossjohann EM, Muschhammer J, Thaden V, Brauneck F, Kischel R, Müller V, Bokemeyer C, Fiedler W, et al. Targeting the TIGIT-PVR immune checkpoint axis as novel therapeutic option in breast cancer. Oncoimmunology. 2019;8(12): e1674605.
24. Rodriguez-Abreu D, Johnson ML, Hussein MA, Cobo M, Patel AJ, Secen NM, Lee KH, Massuti B, Hiret S, Yang JCH, et al. Primary analysis of a randomized, double-blind, phase II study of the anti-TIGIT antibody tiragolumab (tira) plus atezolizumab (atezo) versus placebo plus atezo as first-line (1L) treatment in patients with PD-L1-selected NSCLC (CITYSCAPE). J Clin Oncol. 2020;38:9503-9503.
25. Harjunpaa H, Guillerey C. TIGIT as an emerging immune checkpoint. Clin Exp Immunol. 2020;200:108–19.
26. Swindells MB, Porter CT, Couch M, Hurst J, Abhinandan KR, Nielsen JH, Machindoe G, Hetherington J, Martin ACR . abYsis: Integrated antibody sequence and structure-management, analysis, and prediction. J Mol Biol. 2017;429:356–64.
27. Wu TT, Kabat EA. An analysis of the sequences of the variable regions of Bence Jones proteins and myeloma light chains and their implications for antibody complementarity. J Exp Med. 1970;132:211–50.
28. Krissinel E, Henrick K. Inference of macromolecular assemblies from crystalline state. J Mol Biol. 2007;372:774–97.
29. Zhang Q, Bi J, Zheng X, Chen Y, Wang H, Wu W, Wang Z, Wu Q, Peng H, Wei H, et al. Blockade of the checkpoint receptor TIGIT prevents NK cell exhaustion and elicits potent anti-tumor immunity. Nat Immunol. 2018;19:723–32.
30. Joller N, Lozano E, Burkett PR, Patel B, Xiao S, Zhu C, Xia J, Tan TG, Sefik E, Yajnik V, et al. Treg cells expressing the coinhibitory molecule TIGIT selectively inhibit proinflammatory Th1 and Th17 cell responses. Immunity. 2014;40:569–81.
31. Levin SD, Taft DW, Brandt CS, Bucher C, Howard ED, Chadwick EM, Johnston J, Hammond A, Bontadelli K, Ardourel D, et al. Vstm3 is a member of the CD28 family and an important modulator of T-cell function. Eur J Immunol. 2011;41:902–15.
32. Kurtulus S, Sakuishi K, Ngiow SF, Joller N, Tan DJ, Teng MWL, Smyth MJ, Kuchroo VK, Anderson AC . TIGIT predominantly regulates the immune response via regulatory T cells. J Clin Invest. 2015;125:4053–62.
33. Stanietsky N, Rovis TL, Glasner A, Seidel E, Tsukerman P, Yamin R, Enk J, Jonjic S, Mandelboim O . Mouse TIGIT inhibits NK-cell cytotoxicity upon interaction with PVR. Eur J Immunol. 2013;43:2138–50.

34. Morillon YM, Sabzevari A, Schlom J, Greiner JW. The development of next-generation PBMC humanized mice for preclinical investigation of cancer immunotherapeutic agents. Anticancer Res. 2020;40:5329–41.
35. Zhang JB, Huang Y, Xi G, Zhang FM. HX008: a humanized PD-1 blocking antibody with potent antitumor activity and superior pharmacologic properties. Mabs-Austin. 2020;12(1):1724751.
36. Chen X, Song XM, Li K, Zhang T. Fc gamma R-binding is an important functional attribute for immune checkpoint antibodies in cancer immunotherapy. Front Immunol. 2019;10:292.
37. Alteber Z, Kotturi MF, Whelan S, Ganguly S, Weyl E, Pardoll DM, Hunter J, Ophir E . Therapeutic targeting of checkpoint receptors within the DnAM1 axis. Cancer Discov. 2021;11:1040–51.
38. Serganova I, Moroz E, Cohen I, Moroz M, Mane M, Zurita J, Shenker L, Ponomarev V, Blasberg R . Enhancement of PSMA-directed CAR adoptive immunotherapy by PD-1/PD-L1 blockade. Mol Ther-Oncolytics. 2017;4:41–54.
39. Fang Y, Zhang YJ, Guo CX, Chen CM, Gao HX, Zhou XM, Liu T, Qian Q . Safety and efficacy of an immune cell-specific chimeric promoter in regulating anti-PD-1 antibody expression in CAR T cells. Mol Ther-Meth Clin D. 2020;19:14–23.
40. Gargett T, Yu WB, Dotti G, Yvon ES, Christo SN, Hayball JD, Lewis ID, Brenner MK, Brown MP . GD2-specific CAR T cells undergo potent activation and deletion following antigen encounter but can be protected from activation-induced cell death by PD-1 blockade. Mol Ther. 2016;24:1135–49.
41. Yoon A, Lee S, Lee S, Lim S, Park YY, Song E, Kim DS, Kim K, Lim Y . A novel t cell-engaging bispecific antibody for treating mesothelin-positive solid tumors. Biomolecules. 2020;10(3)399.
42. Kabsch W. Integration, scaling, space-group assignment and post-refinement. Acta Crystallogr D Biol Crystallogr. 2010;66:133–44.
43. Adams PD, Afonine PV, Bunkoczi G, Chen VB, Davis IW, Echols N, Headd JJ, Hung LW, Kapral GJ, Grosse-Kunstleve RW, et al. PHENIX: a comprehensive Python-based system for macromolecular structure solution. Acta Crystallogr D. 2010;66:213–21.
44. Emsley P, Lohkamp B, Scott WG, Cowtan K. Features and development of Coot. Acta Crystallographica Section D-Biological Crystallography. 2010;66:486–501.